Published in partnership with CECCR at King Abdulaziz University



https://doi.org/10.1038/s41612-024-00795-y

Spatially compounding flood-nocturnal heat events over adjacent regions in the Northern Hemisphere

Check for updates

Ruidan Chen^{1,2} ⊠, Jianbin Liu¹, Siao Tang¹ & Xiaogi Li¹

Compound events have become more frequent and diverse under global warming. This study specifically focuses on a type of compound events termed spatially compounding flood-nocturnal heat events over adjacent regions. Five flood hotspots are identified to compound with adjacent nocturnal heat. The flood and nocturnal heat are linked via a water vapor transport belt, with flood over the region of prominent water vapor convergence and ascending anomalies and nocturnal heat over the extension region with moderately increased humidity and weak vertical motion anomaly. The compound events for all the hotspots occur more frequently recently, with commonly positive contribution from the increasing trends of nocturnal temperature (T_N) but various contribution from the trends of precipitation (Pr) and Pr-T_N correlation. The positive contribution of enhanced Pr-T_N correlation results from the enhanced variability of the circulation accompanied with water vapor transport. This study highlights the influence of atmospheric circulation variability on compound events.

A novel type of compound events termed spatially compounding flood-heat over adjacent regions has come to attention during the disastrous summer of 2020 in eastern China $^{1-3}$. During June–July 2020, the mid-lower reaches of the Yangtze River Valley (YRV) witnessed record-breaking precipitation while South China, to the south of YRV, suffered from unprecedented extreme high temperature 1 . Existing literature describe the heat in South China during this event in a broad sense without prescribing the timing of the high temperature $^{1-3}$. In fact, both the June–July mean daily maximum temperature ($T_{\rm X}$) and daily minimum temperature ($T_{\rm N}$) in South China were record-breaking in 2020. However, using the detrended data during the past decades, we found that it is the $T_{\rm N}$ in South China, rather than $T_{\rm X}$, presenting significant correlation with the precipitation (Pr) in YRV. The current study aims at revealing the dynamics leading to the couple of disasters from the perspective of statistic, and thus specifically focuses on the spatially compounding flood-nocturnal heat.

The spatially compounding flood-nocturnal heat events could pose considerable adverse impacts on the society in many aspects. For the 2020 event in eastern China, the flood resulted in at least 129 people dead or missing ^{1,3} and the nocturnal heat greatly threatens the human health via inducing heat-related diseases (http://news.weather.com.cn/2020/05/3322913. shtml). According to the reports of China Power, the YRV flood brings serious damage to the electric supply system (http://

www.chinapower.com.cn/dww/jdxw/20200927/31081.html) while the South China nocturnal heat leads to a record-high demand of electric supply (http://www.chinapower.com.cn/dww/jdxw/20200806/26850. html). Besides, more than 3579.8 thousand hectares of crop areas are affected by the YRV flood (https://www.cma.gov.cn/2011xwzx/ 2011xmtjj/202101/t20210104_569543.html) and the rice planting in South China, a major source of rice yield in China, is supposed to be threatened by the record-breaking nocturnal heat⁴. Besides the 2020 event in eastern China, similar compounding flood-nocturnal heat events are also observed in other regions. For instance, the National Climate Report released by the National Centers for Environmental Information (https://www.ncei.noaa.gov/access/monitoring/monthlyreport/national) documented some examples in the US. In July 2021, Arizona in the southwestern US witnessed unprecedented Pr, while to its northwest, California had the hottest July. In July 2022, Missouri and Kentucky in the middle eastern US experienced historic Pr, while the adjacent southern Plains region saw temperature well above normal. Particularly, the high temperature in these two events feature recordbreaking nighttime temperature. Compared to isolated occurrences, the concurrent flood and nocturnal heat may cause disproportionate impacts such as raising fatalities, amplifying the pressure on infrastructure and causing multiple harvest failures. Hence, it is essential to

¹School of Atmospheric Sciences and Guangdong Province Key Laboratory for Climate Change and Natural Disaster Studies, Sun Yat-sen University, and Southern Marine Science and Engineering Guangdong Laboratory (Zhuhai), Zhuhai, China. ²Key Laboratory of Tropical Atmosphere–Ocean System, Ministry of Education, Zhuhai, China. ⊠e-mail: chenrd3@mail.sysu.edu.cn

unveil the changes and influencing factors of spatially compounding flood-nocturnal heat events, especially under the background of climate change.

The correlation between the relevant variables is a critical factor determining the likelihood of compound events, with considerably higher likelihood for significantly correlated variables⁵⁻⁸. For this reason, some studies take the variable dependence as a necessary requirement when defining compound events^{5,7}. Previous studies used the T_X in South China to analyze the 2020 compound event and found that the extremes over YRV and South China were modulated by the same modulator, namely, the intensified western Pacific subtropical high. However, the weak correlation between the T_X in South China and the Pr in YRV means that these two variables are not dynamically coupled from the perspective of statistic, and their joint extremes are more likely random if the trends relating to climate change are removed. In contrast, the significant relationship between the T_N in South China and the Pr in YRV renders their joint extremes including the 2020 case. Moreover, as T_N increases obviously faster than T_X under global warming⁹⁻¹¹, compounding flood-nocturnal heat are expected to be more disastrous than flood-daytime heat. Nocturnal heat greatly threatens the humans in the regions not accessible to air conditioner, such as the poor areas and the mid-latitudes that used to be seldomly affected by high temperature. Even in the regions accessible to air conditioner, the elders, who are vulnerable to disease, are often unwilling to use the air conditioner due to economic reason or reduced perception of heat. Once exposed, the humans' health is more threatened by the nocturnal heat than daytime heat 12,13. Therefore, it is important to understand the spatially compounding floodnocturnal heat events.

Starting from the 2020 incident in China, this study makes further efforts to discover the hotspots of summer flood that spatially compounding with adjacent nocturnal heat in the Northern Hemisphere. The roles of Pr trend, $T_{\rm N}$ trend and the correlation between detrended Pr and detrended $T_{\rm N}$ are analyzed to understand the changes in the frequency of compound events under climate change. Many previous studies have revealed that $T_{\rm N}$ in most regions of the world present prominent increasing trends while Pr present different regional trends $^{14-16}$. In contrast, the relationship between Pr and $T_{\rm N}$ over adjacent regions is rarely addressed. Moreover, the relationship between variables might vary under climate change, raising a great challenge in understanding and projecting the changes in compound events $^{17-19}$. In this study, the atmospheric dynamics responsible for the intrinsic correlation between relevant variables and its change are specifically analyzed.

Results

Compound events in eastern China

The 2020 summer case in eastern China is firstly analyzed. Figure 1 demonstrates the extremes of flood in YRV and nocturnal heat in South China during June–July 2020. The anomalies of Pr in YRV and T_N in South China both exceed 2.5 standard deviations in their centers, with numerous stations featuring anomalies ranking among top three since 1961 (Fig. 1a). The mean Pr and T_N anomalies over the key regions of YRV 105°E-122°E, 28°N-34°N (YRV-Pr) and South China 105°E-120°E, 20°N-27°N (SC-T_N) reach 3.7 and 3.1 standard deviations, respectively, both breaking the records during the past 60 years (Fig. 1b). Defining compound events as both the Pr and $T_{\rm N}$ anomalies exceeding 1 standard deviation, four summers stand out, including 1998, 2015, 2016 and 2020. All the four summers occur after the early 1990s, which are contributed by the significant increasing trends of both Pr and T_N. After removing the trends related to climate change, the detrended residuals are analyzed to reveal the influence of atmospheric circulation alone (see Methods). The detrended YRV-Pr and SC-T_N have a significant correlation coefficient of 0.54, contributing to their concurrent extremes. Four summers (1983, 1998, 2016, 2020) appear as detrended compound events (Fig. 1c), which also occur more frequently after the early 1990s. This is related to the enhanced relationship between the two variables during the past decades, with significant (mostly insignificant) correlation coefficient after (before) the early 1990s (Fig. 1d). Therefore, the

frequency trend of compound events is modulated by the trends of the two involved variables and their correlation coefficient, all of which are important for the compounding flood-nocturnal heat events in YRV and SC. Compared to SC-T $_{\rm N}$, SC-T $_{\rm X}$ is insignificantly correlated with YRV-Pr after removing their trends (r = 0.16), which means the flood-daytime heat over YRV and SC is not statistically coupled if only the atmospheric circulation variability is considered.

To understand the dynamical linkage between YRV-Pr and SC-T_N, the circulation anomalies associated with their compound events are analyzed. In the 2020 summer, a remarkable anticyclonic anomaly occurs over the northwestern Pacific in both the mid and lower troposphere (Fig. 2a, b). In its western part in the lower troposphere, anomalous southeasterly blows from the South China Sea toward the coast, turns into southwesterly over SC and then into westerly over YRV. These wind anomalies delivery abovenormal water vapor from the South China Sea to the land, which passes SC and mainly converges over YRV. The convergence causes not only anomalous high humidity but also anomalous ascent over YRV, leading to flood in situ. The above processes are consistent with previous study¹. On the other hand, SC is located in the southern extension of the high humidity belt, presenting moderately positive humidity anomaly. Meanwhile, the vertical motion over SC features weak descending anomaly, enabling the moderately increased water vapor stays in the atmosphere. The increased water vapor over SC could efficiently inhibit the outgoing longwave radiation cooling, favoring the formation of nocturnal heat^{20–22}. Thereby, the compounding flood-nocturnal heat over YRV and SC is linked by the abnormal southwesterly water vapor transport belt traversing the two regions. The convergence zone of water vapor, featuring strong positive humidity and ascent anomalies, leads to flood, while the extension zone of the positive humidity center, featuring moderately positive humidity and weak vertical motion anomalies, leads to nocturnal heat. These anomalies change little if the long-term trends are removed (Supplementary Fig. 1), suggesting the dominate role of atmospheric circulation variability in the anomalies. Composite analyses (Fig. 2c, d) and individual circulation pattern (Supplementary Fig. 1) of the detrended compound events also gain similar results, indicating the above-proposed dynamical processes are robust and generally apply to the compound events over YRV and SC.

Different from SC- T_N , SC- T_X is not correlated with YRV-Pr due to the distinct physical processes influencing T_N and T_X and the different roles of water vapor in T_N and T_X anomalies. Increased T_N is mainly due to the inhibition of longwave radiation cooling, while increased T_X is largely contributed by the enhanced solar radiation at surface. Water vapor could not only increase the downward longwave radiation but also favor more cloud cover and thus diminish the insolation. During daytime, these two effects counteract each other and leads to weak T_X anomaly. At night, only the longwave radiation effect exists and results in significant T_N anomaly. These processes leading to better Pr- T_N correlation than Pr- T_X correlation are confirmed by the composite anomalies of relevant variables for YRV-Pr events (Supplementary Fig. 2). Indeed, the composite of YRV-Pr events show much more significant increase of T_N than T_X over SC, accompanied by increased water vapor, cloud cover, downward longwave radiation and decreased downward shortwave radiation.

Another issue is that the dynamical linkage between the flood and adjacent nocturnal heat experiences an interdecadal change, which manifests the modulation of atmospheric circulation variability on the frequency trend of compound events. In order to investigate the causes of the interdecadal change in the linkage, composite analyses are performed separately for the detrended abnormal YRV-Pr events and SC-T $_{\rm N}$ events, both before the interdecadal change (insignificantly correlated period; denoted as P1) and afterwards (significantly correlated period; denoted as P2). During P2, for both abnormal YRV-Pr and SC-T $_{\rm N}$ events, the composite anomalies are similar to those presented in Fig. 2c, d (Supplementary Fig. 3c, d, g, h). During P1, albeit abnormal YRV-Pr and SC-T $_{\rm N}$ events are still associated with an anticyclonic anomaly, the southwesterly anomalies are obviously weaker than those during P2 and result in weaker humidity anomalies (Supplementary Fig. 3a, b, e, f). Quantitatively, the averaged southwesterly

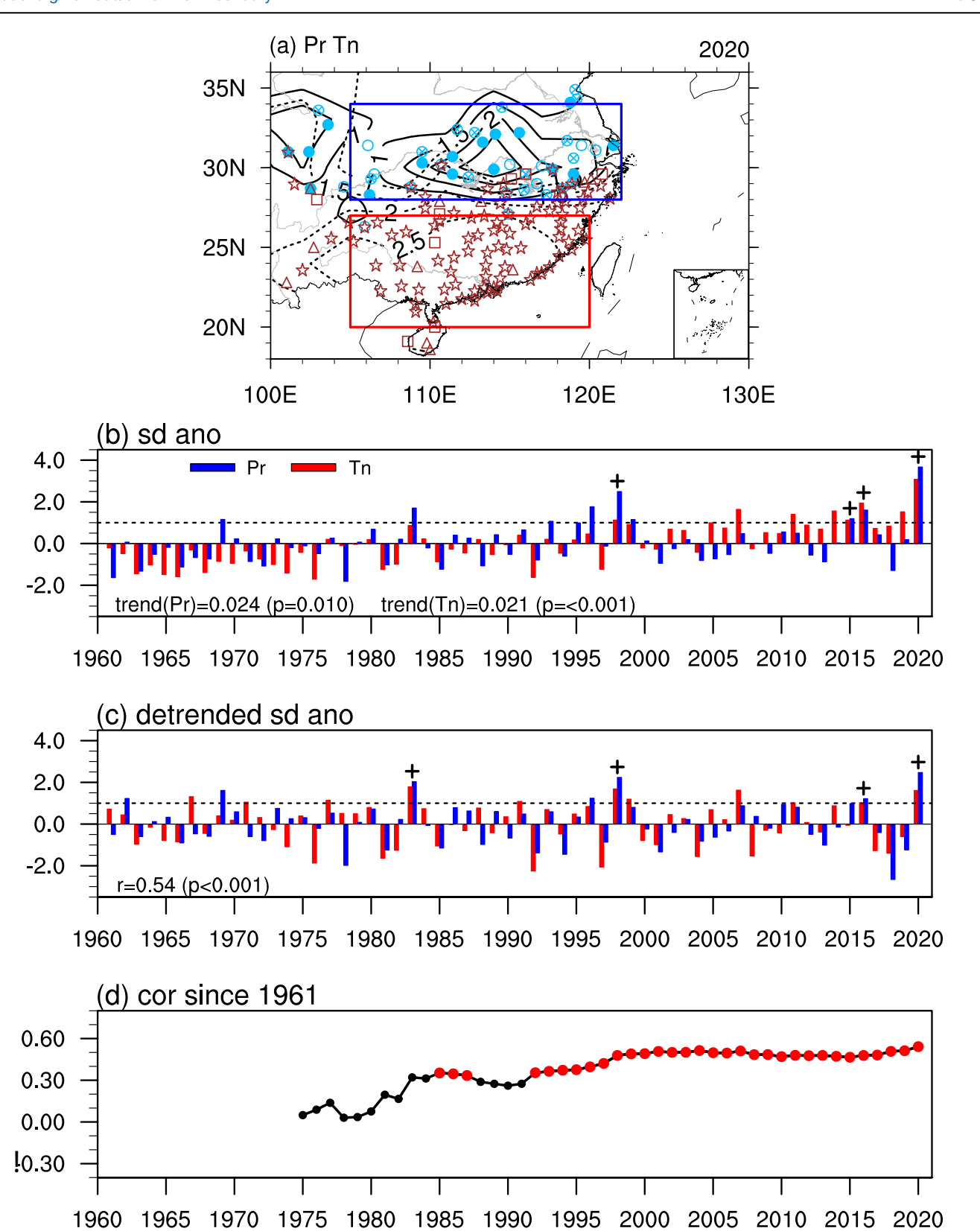


Fig. 1 | Statistics of the compound events in eastern China. a Standardized anomalies of Pr (solid contours) and T_N (dashed contours) in eastern China during June–July 2020. Blue solid circles, circles with crosses and hollow circles denote precipitation ranking the first, second and third since 1961, respectively. Red stars, squares and triangles denote T_N ranking the first, second and third since 1961,

respectively. Time series of (b) standardized anomalies and (c) standardized detrended anomalies of YRV-Pr (blue bars) and SC- $T_{\rm N}$ (red bars) during 1961 to 2020. Black crosses over the bars mark the compound events. d Correlation coefficients between detrended YRV-Pr and SC- $T_{\rm N}$ since 1961 to sliding end years. Red dots denote significant correlation coefficients.

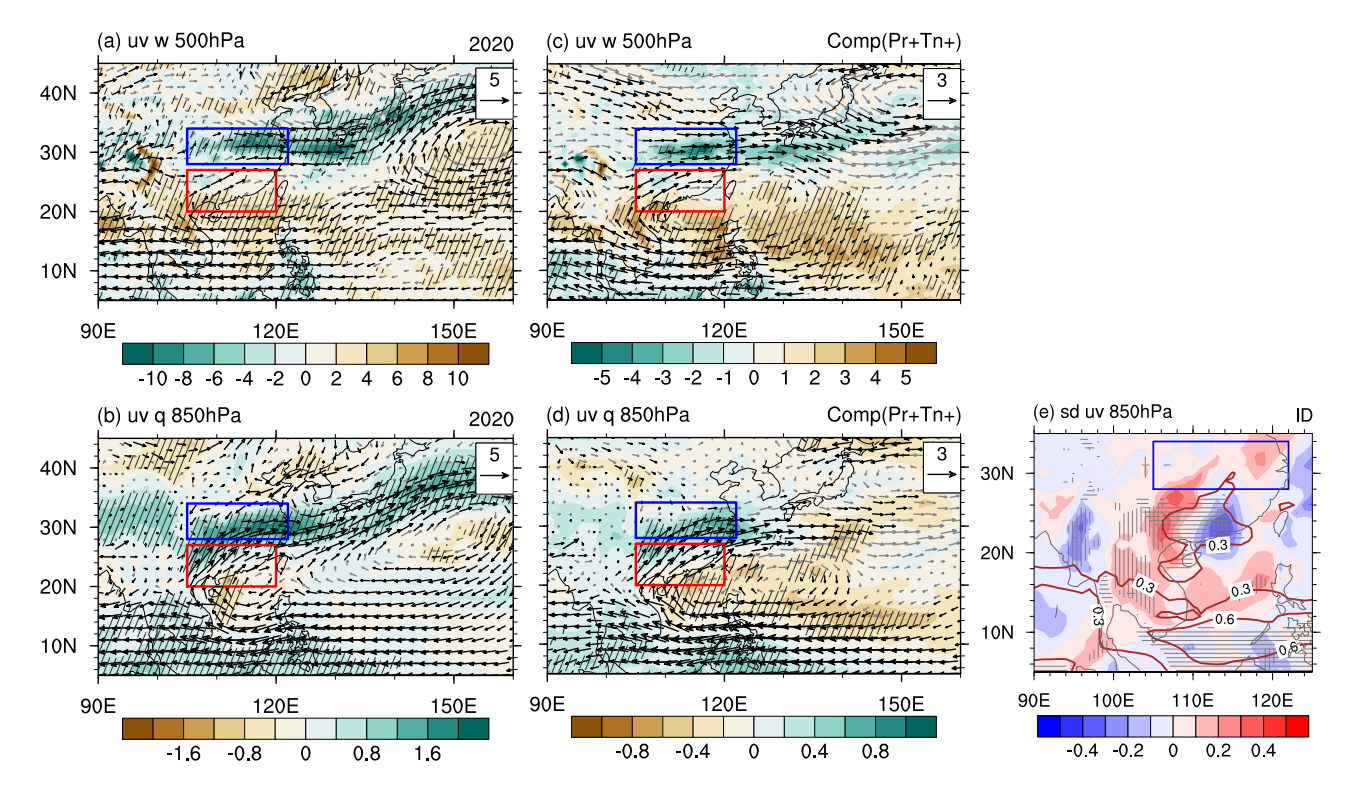


Fig. 2 | Atmospheric circulation associated with the compound events in eastern China. Anomalies of ($\bf a$, $\bf c$) 500-hPa horizontal wind (vectors; units: m s⁻¹) and vertical velocity (shadings; units: 10^{-4} hPa s⁻¹), ($\bf b$, $\bf d$) 850-hPa horizontal wind (vectors) and specific humidity (shadings; units: g kg⁻¹) for the ($\bf a$, $\bf b$) 2020 summer (slashes mark the shading areas with anomalies larger than 1 standard deviation) and ($\bf c$, $\bf d$) composite of detrended compound events during 1961 to 2020 (slashes mark

the significant shading areas). **e** Interdecadal changes in the interannual standard deviations of 850-hPa meridional (shadings; vertical lines mark the significant areas) and zonal (contours; horizontal lines mark the significant areas) winds around the early 1990s. The blue and red boxes denote the key regions of YRV and SC, respectively.

over SC increases from $0.60~{\rm m~s^{-1}}$ in P1 to $1.44~{\rm m~s^{-1}}$ in P2 ($0.91~{\rm m~s^{-1}}$ in P1 to $1.14~{\rm m~s^{-1}}$ in P2) for abnormal YRV-Pr (SC-T_N) events. The weakened southwesterly anomaly diminishes the dynamical linkage between YRV-Pr and SC-T_N, resulting in their insignificant correlation during P1. In essence, the interdecadal changes in the composite wind anomalies are related to the changes in the wind variability. The meridional (zonal) wind presents an interdecadal enhanced variability over western South China (South China), composing the enhanced variability of the southwesterly linking YRV and South China (Fig. 2e). The enhanced variability of the southwesterly not only strengthens the dynamical linkage between YRV-Pr and SC-T_N, but also results in more frequent large-amplitude anomalies favoring the compound events.

Flood hotspots compounding with adjacent nocturnal heat in the Northern Hemisphere

An interesting and important issue is whether the compound events found in eastern China take place in other regions. We start by identifying the summer flood hotspots manifested as large Pr variability centers, and then check their relationship with the T_N in surrounding regions. Large variability of raw precipitation (Fig. 3a) and detrended precipitation (Supplementary Fig. 4a) in the Northern Hemisphere continent both occurs over: (1) the East Asian monsoon region, with centers over YRV, South China and Northeast Asia (denoted as EA-YRV, EA-SC, EA-NEA); (2) the Southeast Asian monsoon region, with centers over Indochina Peninsula and the northern Philippines (denoted as SEA-IP, SEA-NPh); (3) the South Asian monsoon region with a center over northeastern India (denoted as SA-NEIn); (4) the United State with centers over the Great Plains and the southeastern coast (denoted as US-GP, US-SE); (5) the North American monsoon regions with a center over the Central American isthmus (denoted as CAm)²³; (6) the northern South America (denoted as SAm); (7) the North African monsoon region (denoted as NAf). The above flood centers are consistent with the centers of mean precipitation revealed by previous studies^{24,25}. Among these centers, the Pr over EA-YRV, SA-NEIn, US-GP, CAm and NAf show significant correlation with the T_N in adjacent region (Fig. 3b-f), while the other centers show no significant correlation with adjacent T_N (Supplementary Fig. 5). Therefore, the former five centers are selected as flood hotspots that dynamically coupled with adjacent nocturnal heat. The flood over EA-YRV is coupled with the nocturnal heat over South China, SA-NEIn with northwestern Tibetan Plateau (only the region with altitude greater than 3000 m is considered; Supplementary Fig. 4b), US-GP with southeastern coast of US, CAm with northern South America and NAf with northeastern Africa (Fig. 3b-f). The frequency of compounding floodnocturnal heat events and the modulation of long-term trends and atmospheric dynamics are examined for the five hotspots. The results for EA-YRV based on GPCP Pr and ERA5 TN data are basically consistent with those presented in the previous section (Supplementary Figs. 6 and 7), ensuring the quality of global Pr and T_N data. Only the analyses of the rest four hotspots are presented in the follows.

Figure 4 demonstrates the temporal evolution of Pr, T_N and their correlation for each hotspot. Identified by the original Pr and T_N anomalies, there are five compound events for SA-NEIn, four for US-GP, four for CAm and one for NAf, all of which occur more frequently in recent decades (Fig. 4a1–a4). The T_N in all adjacent key regions present significant increasing trends, making positive contribution to the increasing trends of compound events. In contrast, the Pr trends vary among hotspots, with significant decreasing trends and negative contribution in CAm and NAf while insignificant trends in SA-NEIn and US-GP.

The correlation between detrended Pr and T_N is robustly significant for CAm and NAf, while exhibits an interdecadal enhancement around the late 1970s for SA-NEIn and around the mid-1980s for US-GP (Fig. 4c1–c4). For the latter two hotspots, the enhanced correlation contributes to the more occurrence of detrended compound events after the corresponding

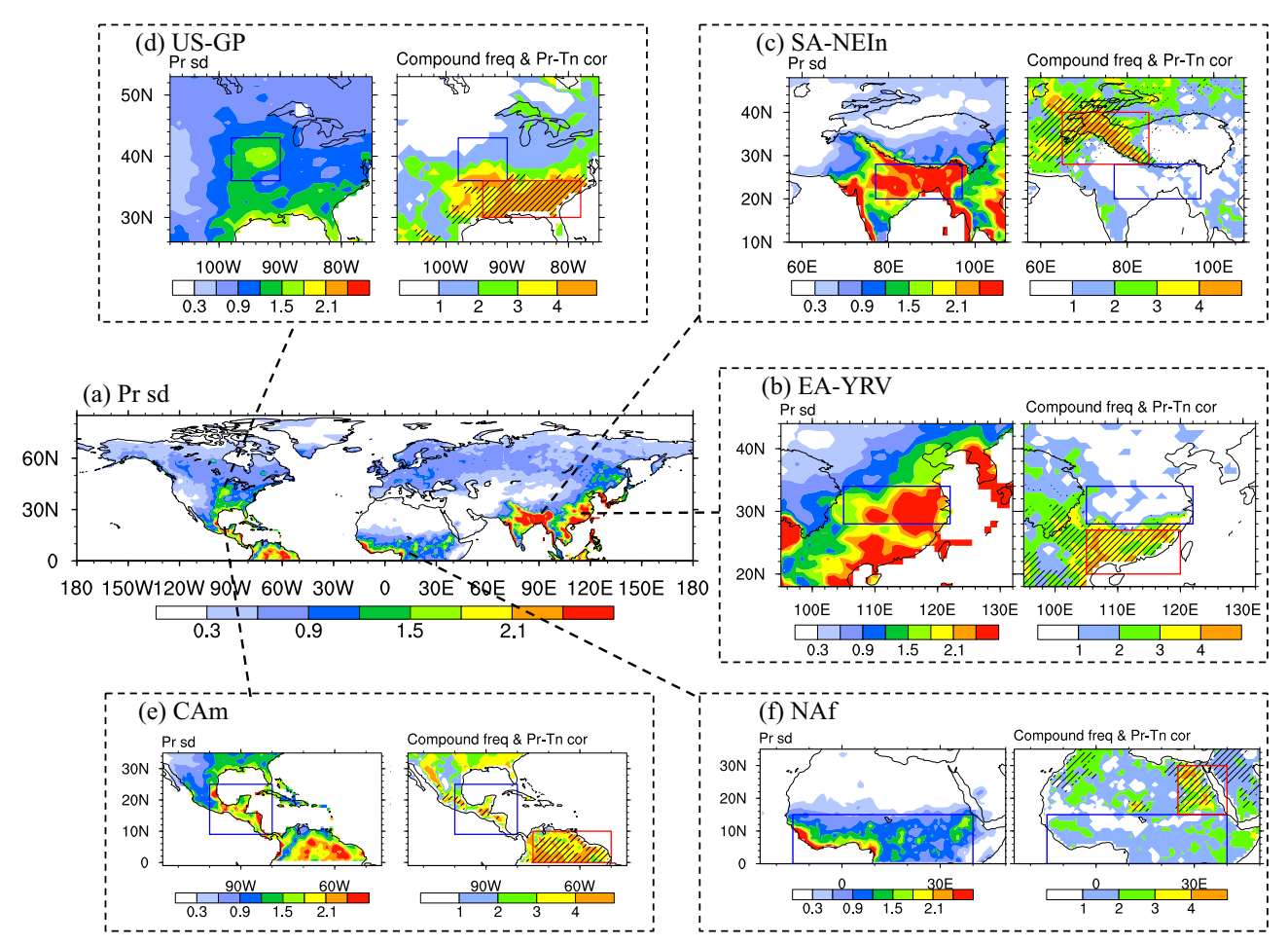


Fig. 3 | Hotspots of compound events in the Northern Hemisphere. a Spatial distribution of summer Pr standard deviation in the Northern Hemisphere (unit: mm d^{-1}). b-f (left plots) Zooming Pr standard deviations over the five flood hotspots compounding with adjacent nocturnal heat and (right plots) frequencies of compound events between flood over the key regions of hotspots and nocturnal heat over

the adjacent grids (shadings). Slashes mark the grids with detrended T_N significantly correlated with the detrended Pr averaged over the key regions of flood hotspots. Blue and red boxes denote the selected key regions of flood and nocturnal heat for the compound events, respectively.

interdecadal change (Fig. 4b1, b2). It is noted that the $Pr-T_N$ correlation coefficient for US-GP only enhances slightly around the mid-1980s, but it changes from insignificant to significant due to the increased sample size and indicates a more stable relationship recently. We are cautious that in statistics, a very weak correlation can be significant providing the sample size is large enough. In this study, the smallest significant correlation coefficient is above 0.3, which is not very weak and the corresponding p value is smaller than 0.01, suggesting the significant correlation coefficients are reliable.

Composite analyses of the atmospheric circulation anomalies for the detrended compound events in all hotspots are demonstrated in Fig. 5. Similar to EA-YRV, a water vapor transport belt connecting the two adjacent key regions is critical for the compound events for all hotspots, but presenting distinct features and embedded in different circulation systems.

For SA-NEIn, an anomalous westerly belt prevails over the Arabian Sea and turns into southwesterly around the northwestern coast of India in the lower troposphere (Fig. 5b1). The anomalous westerly and southwesterly strengthen the South Asian summer monsoon and bring in abundant water vapor, which is vital for the NEIn flood. Meanwhile, an anomalous cyclone dominates over NEIn, which not only enables in-situ active ascent but also delivers the water vapor further northwestward via the southeasterly in its eastern edge (Fig. 5a1, b1). On the other hand, an anomalous anticyclone is centered to the northwest of the Tibetan Plateau in the mid and upper troposphere (Figs. 5a1 and Supplementary Fig. 8a), which might be the thermal vorticity adaption to the diabatic heating associated with NEIn Pr^{26,27}. The anomalous easterly in the southern edge of the anticyclone could

transport the climatological moister air over the eastern Plateau to the western Plateau (Supplementary Fig. 8b). Consequently, obviously abovenormal water vapor occurs over the northwestern Tibetan Plateau (Fig. 5a1) and favors the nocturnal heat via greenhouse effect.

For US-GP, the circulation anomaly shows a vigorous anticyclone over the southeastern US (Fig. 5a2, b2). In the western part of the lower-tropospheric anticyclone, anomalous southwesterly prominently enhances the GP low-level jet²⁸ and brings in abundant water vapor to the key regions of both Pr and T_N (Fig. 5b2). In the mid troposphere, the GP key region is dominated by significant ascent in the northwest of the anticyclone while the southeastern coast key region by descent in the anticyclonic center, favoring increased Pr and T_N , respectively.

For CAm, there is significant lower-tropospheric southwesterly extending from the eastern tropical Pacific to CAm, which is embedded in the cross-equatorial flow from the southeastern tropical Pacific (Fig. 5b3). The anomalous southwesterly strengthens the North American summer monsoon and results in significantly increased humidity over CAm, which together with ascending anomaly favor above-normal Pr (Fig. 5a3, b3). On the other hand, moderately increased humidity extending from the westerly belt dominates over the northern South America and favors increased $T_{\rm N}$.

For NAf, an anomalous low-level southwesterly belt extends from the tropical Atlantic to NAf, which is associated with the cross-equatorial flow from the southwestern tropical Atlantic and strengthens the NAf monsoon (Fig. 5b4). Meanwhile, a cyclonic anomaly appears over the subtropical North Atlantic and induces stronger westerly entering NAf (Fig. 5a4, b4).

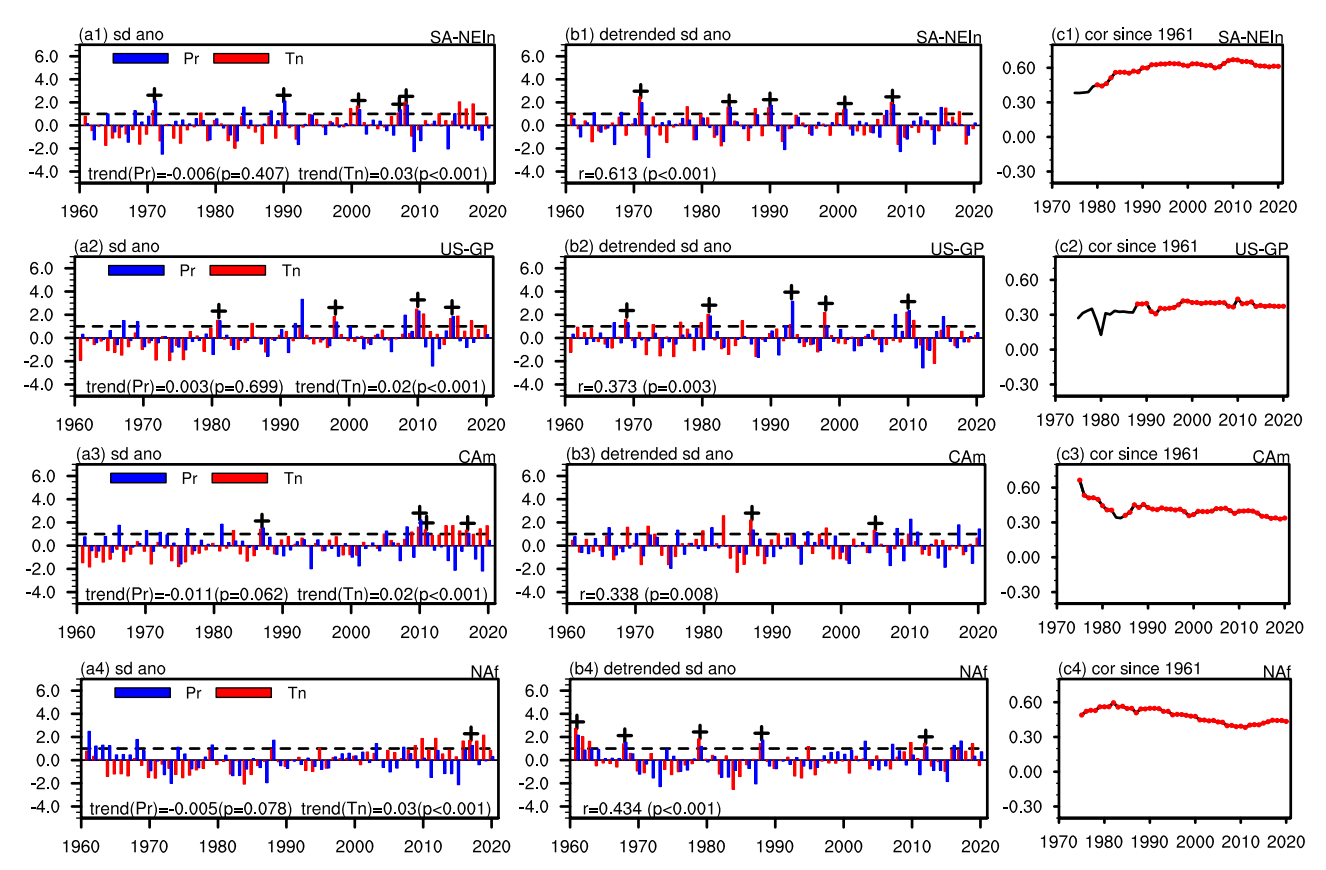


Fig. 4 | Statistics of the compound events in the Northern Hemisphere hotspots. Same as Fig. 1b-d, but for the averaged Pr of the flood hotspots over (a1-c1) northeastern India in South Asia, (a2-c2) the Great Plains in the US, (a3-c3) the

Central American isthmus, (a4–c4) the North African monsoon region and the averaged $T_{\rm N}$ over the corresponding adjacent nocturnal heat regions.

The abnormal southwesterly and westerly water vapor transport belt leads to above-normal humidity and ascent over NAf. The positive humidity anomaly is centered in the northern boundary. The ascent anomaly, albeit with scattered significant signals, appears over the whole NAf and favors the flood. Meanwhile, the northeastern African key region is dominated by moderately positive humidity anomaly extending from the southwesterly belt, favoring increased $T_{\rm N}$.

For all hotspots, only a few years have Pr and T_N anomalies exceeding 1 standard deviation simultaneously, which is consistent with the low frequency of compound events. Thus, it is reasonable that most years have other combinations of standardized Pr and T_N anomalies with different strengths and polarities (Fig. 4). In order to find out the key processes favoring the synchronous variation of Pr and T_N both exceeding 1 standard deviation, we compare the composites of synchronous years (Pr > 1sd and $T_N > 1$ sd; Figs. 2 and 5) and asynchronous years (Pr > 1sd but $T_N < 1$ sd; Supplementary Fig. 9). It turns out that the key water vapor transport belt identified in the synchronous years changes obviously in the asynchronous years, which becomes weaker for EA-YRV and CAm, disappears for SA-NEIn, shrinks and is unable to reach the key region of adjacent nocturnal heat for US-GP and NAf. Therefore, the positive humidity anomalies are prominently weaker for all regions. It is highlighted that the water vapor transport belt connecting the adjacent regions is essential for the compounding flood-nocturnal heat events.

Furthermore, the interdecadal enhancements of the Pr- T_N correlations for SA-NEIn and US-GP are investigated, via comparing the atmospheric circulation before and after the interdecadal changes. The responsible atmospheric dynamical processes are found to be similar to those for EA-YRV. On the one hand, the composites of Pr events and T_N events both show weaker anomalies in P1 than in P2 (Supplementary Figs. 10 and 11). The weakening of the water vapor transport belt diminishes the coupling of

Pr and T $_{\rm N}$ in adjacent regions in P1. On the other hand, the circulation associated with the water vapor transport belt presents an interdecadal enhancement in the interannual variability. For SA-NEIn, the lower-tropospheric wind displays obviously enhanced variability extending from the northern Arabian Sea to northern India (over the northwestern coast of India) for the zonal (meridional) component (Fig. 5c1). For US-GP, the lower-tropospheric wind variability exhibits significant enhancement in the zonal (meridional) component right over the southern and northern (western and eastern) edges of the composite anticyclone (Fig. 5c2). The enhanced circulation variability in P2 strengthens the Pr-T $_{\rm N}$ linkage and favors the more occurrence of strong Pr and T $_{\rm N}$ anomalies.

Obviously, the timing of interdecadal change differs for EA-YRV, SA-NEIn and US-GP, which might be due to the distinct forcing of tropical SST. For East Asia, its climate is remarkably influenced by the tropical Pacific SST. The interdecadal enhanced wind variability over South China around the early 1990s might be related to the enhanced influence of ENSO. After the early 1990s, the ENSO cycle presents a more rapid evolution and an obvious La Niña pattern forms in the summer after El Niño peak^{29,30}, favoring an anomalous anticyclone over the northwestern Pacific with southwesterly over South China²⁹. For SA-NEIn, the interdecadal enhancement of wind variability over the North Indian Ocean is possibly related to the modulation of the tropical Indian Ocean SST. After the late 1970s, the SST variability increases over the tropical Indian Ocean, which would enhance the influence of SST anomaly on the atmosphere over the North Indian Ocean³¹. As for the US, the SST over both the tropical Atlantic and eastern tropical Pacific could influence the GP via inducing an anomalous anticyclone and associated southwesterly over the southeastern US³². Since the mid-1980s, the relationship between the SST over the tropical Atlantic and eastern tropical Pacific intensifies significantly³³, which could exert a synchronous effect to enhance the relevant atmospheric variability.

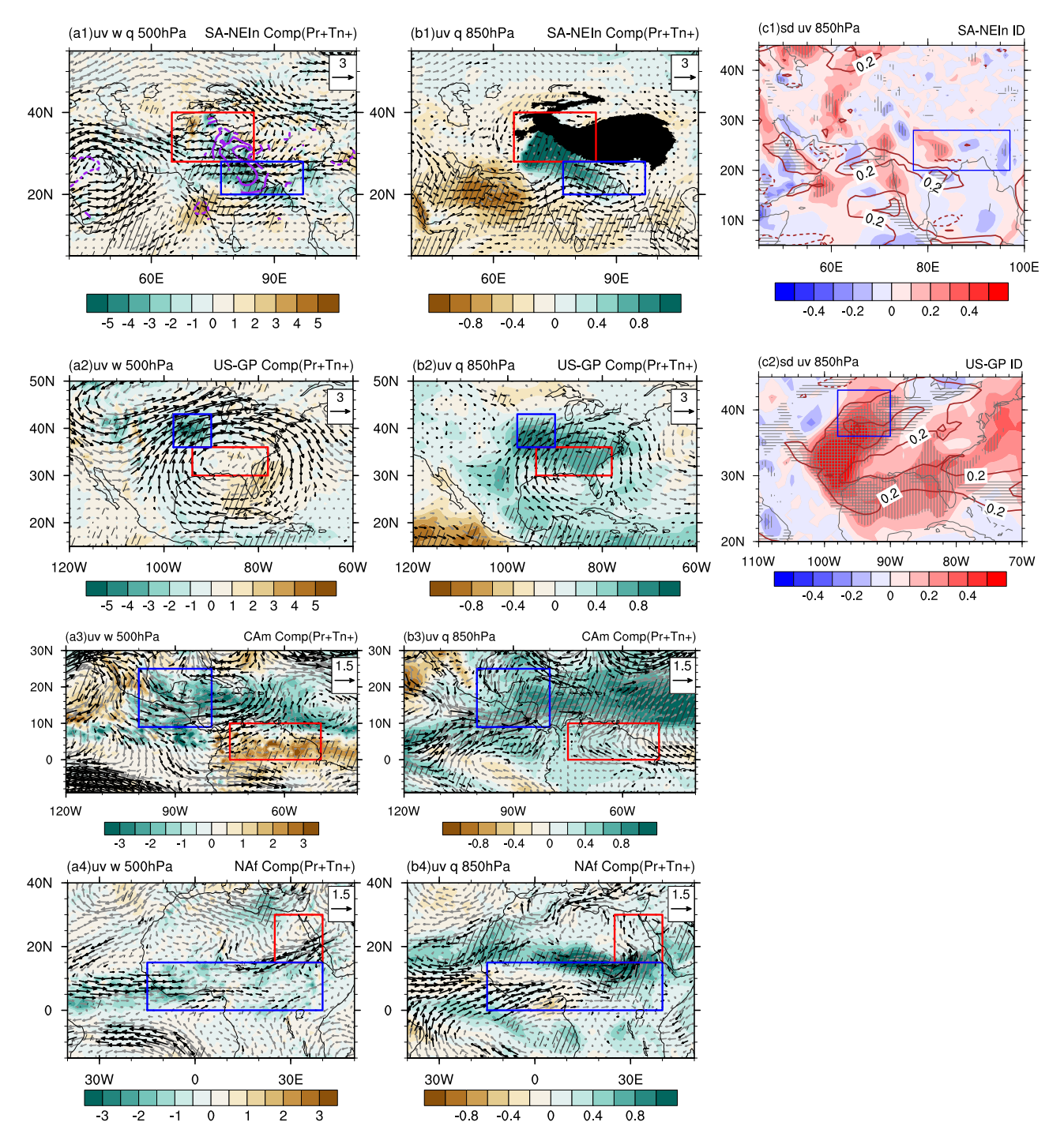


Fig. 5 | Atmospheric circulation associated with the compound events in the Northern Hemisphere hotspots. (Left two columns) Same as Fig. 2c, d, but for the detrended compound events between the flood over $(\mathbf{a}\mathbf{1}-\mathbf{b}\mathbf{1})$ northeastern India in South Asia (purple contour in $\mathbf{a}\mathbf{1}$ additionally shows the significant 500-hPa specific humidity anomaly aloft the terrain; units: \mathbf{g} kg $^{-1}$; intervals: 0.2 g kg $^{-1}$; the Tibetan Plateau is outlined at 500 hPa and shaded with black at 850 hPa), $(\mathbf{a}\mathbf{2}-\mathbf{c}\mathbf{2})$ the Great

Plains in the US, (a3-c3) the Central American isthmus, (a4-c4) the North African monsoon region and the adjacent nocturnal heat. The blue and red boxes denote the key regions of flood and nocturnal heat, respectively. c1, c2 Same as Fig. 2e but for the interdecadal changes in the wind fields over (c1) South Asia around the late 1970s and (c2) the US around the mid-1980s.

Discussion

Starting from the 2020 disastrous summer in eastern China, this study specifies a type of compound events termed spatially compounding flood-nocturnal heat events over adjacent regions. In the Northern Hemisphere, five flood hotspots are identified to compound with adjacent nocturnal heat, including the floods over EA-YRV, SA-NEIn, US-GP, CAm and NAf compounding with the nocturnal heats over SC, northwestern Tibetan Plateau, southeastern coast of US, northern South America and northeastern

Africa, respectively. The dense population in EA, SA, the US and NAf calls for special attention so as to minimize the shocks of such compound events. Albeit the high-altitude northwestern Tibetan Plateau is rarely inhabited by humans, the fragile ecosystem over this region is greatly threatened by nocturnal heat. The warming may influence the plant species richness, rangeland quality and ecological stability, reducing their ability to provide reliable ecosystem services for humanity^{34–36}. Moreover, the extreme warming may accelerate the glacier retreat and permafrost thawing, causing hydrological

changes on the plateau and in downstream regions³⁷. These negative effects, together with the SA-NEIn flood, pose great threat on the global ecological and hydrological systems and thus also require close attention. It is also noted that the spatially compound events may take place in the same country or across different countries. The occurrences within a country pose considerable pressure on the national emergency response system, demanding multiple departments to properly react to different disasters at the same time. The occurrences across different countries could amplify the damages to the globally interconnected economic and ecological systems.

The likelihood of compound events is remarkably elevated if the relevant variables are significantly correlated, and the compound events concerned here belong to this type. We found a similar underlying dynamic leading to the variables' dependence for all the identified hotspots, that is, the flood and adjacent nocturnal heat are linked via a water vapor transport belt. Flood occurs at the region of prominent water vapor convergence and ascending anomalies along the belt, while nocturnal heat at the extension region with relatively moderately increased humidity and weak vertical motion anomalies. The abundant water vapor lifting provides substantial moist energy for flood, while the moderately increased water vapor in the air would inhibit the outgoing longwave radiation cooling at night and favor nocturnal heat. Considering the critical role of water vapor, the increasing water vapor content under global warming 38,39 could serve as a favorable thermal condition for the occurrence of these compound events.

The variation of compound events under climate change is an issue greatly concerned by multiple shake holders not limiting to the government planners, disaster relief departments and insurance agencies^{5,40}. Our results show that the spatially compounding flood-nocturnal heat events over all the hotspots appear more frequently in recent decades, with commonly positive contribution from the significant increasing trend of T_N but different contribution from the trends of Pr and Pr-T_N correlation. Positive (Negative) contribution from significant Pr increasing (decreasing) trend occurs over EA-YRV (NAf), while positive contribution combined with enhanced Pr-T_N correlation occurs over EA-YRV, SA-NEIn, US-GP and the corresponding adjacent regions. The different regional Pr trends are modulated by the changes in the dynamical processes because the atmospheric moisture content basically increase under global warming^{41,42}. The changes in the correlation coefficients manifest the modulation of climate variability, which is related to the changes in the variability of the circulation accompanied with water vapor transport belt. Enhanced circulation variability would strengthen the Pr-T_N connection and favor their concurrent extremes. It should be mentioned that our method only qualitatively analyzes the contributions of the relevant variables' trends and their correlation variation to the compound events. Quantitative analyses on their relative contributions can be performed using the copula model method^{43,44}. A corresponding preliminary analysis indicates that our qualitative method is consistent with the copula model method (not shown), ensuring the reliability of this study. The current method is chosen due to its convenience to pick out events for analyses of atmospheric dynamics, which is our main purpose.

The results about the dynamical linkage in the spatially compounding events and its variation could advance the understanding of the critical role of atmospheric circulation variability in modulating compound events. The relevant mechanism is investigated mainly via composite analysis, a simple but useful statistical method based on historical observed cases, which could provide factual support for the multiple researches relying on model output^{2,3,6}. Moreover, the importance of atmospheric circulation variability greatly challenges the climate models' proper presentation and projection of these events due to the models' high uncertainty in simulating the atmospheric circulation variability^{45–47}, in turn underscoring the necessity of analyses based on observed data.

Methods

Data

The observation of Pr, T_N and T_X in China are collected from the recently updated 366 stations homogenized daily datasets⁴⁸. Monthly data are obtained by averaging the daily observation. Global Pr is from the Global

Precipitation Climatology Centre (GPCC) that derived from global station data⁴⁹, with a horizontal resolution of $1^{\circ}\times 1^{\circ}$. Global T_N and other atmospheric variables are from the fifth generation of European Centre of Medium Range Weather Forecasts (ERA5) monthly averaged reanalysis data⁵⁰, with a horizontal resolution of $1^{\circ}\times 1^{\circ}$. The analyses focus on June–July, the months when the 2020 compound event in eastern China happened. Besides, choosing June–July could reduce the influence of tropical cyclone, which is the most active in late summer in the Northern Hemisphere. The analyzed period covers 60 years from 1961 to 2020.

Definitions

Compounding flood-nocturnal heat events are defined as the summers with the Pr and $T_{\rm N}$ anomalies over the concerned adjacent regions concurrently exceed 1 standard deviation. Adjacent regions refer to two regions with the nearest distance between their boarders less than 5° latitudes or longitudes. The threshold of 1 standard deviation might be moderate for defining univariate extreme events, but is rigorous for bivariate extreme events. Slight enhancement of the 1 standard deviation threshold does not obviously change the main results (not shown), but 1 standard deviation is adopted to ensure enough sample sizes for the composite analyses for all regions. The frequency of compound events based on this definition is 1/60 to 5/60 for the various analyzed regions in this study (Supplementary Table 1), which is in line with statistical extremes (less than 10%) and meets previously proposed definition 51 .

Statistical methods

According to previous studies^{1,52}, a variable's trend is related to the signal of climate change and the detrended residual could represent the influence of atmospheric circulation alone. In this study, the linear trend is computed to describe the strength of signal related to climate change. Then the detrended residual is extracted using a non-linear trend with a cubic smoothing spline⁵², considering the non-linear evolution of the background climate state^{1,52}. Composite analyses are performed on the detrended residuals to reveal the statistically dynamical linkage between flood and adjacent nocturnal heat. The summers with the detrended anomalies of the two relevant variables both exceeding 1 standard deviation are termed detrended compound events. Abnormal Pr events and T_N events in an individual region denote the summers with corresponding detrended univariate anomalies exceeding 1 standard deviation. Similarities (Discrepancies) between the individual-region abnormal events and compound events highlight the factors favorable (unfavorable) for the spatially compounding, which help understanding the interdecadal change in the internal linkage. The years used for composite analyses are listed in Supplementary Table 1, including during the whole period and different decades. Student's t test with a significant level of 90% is utilized to assess the composite results. The dependence between flood and nocturnal heat is evaluated by the Pearson correlation coefficient between the detrended June-July averaged annual time series of Pr and T_N over the adjacent regions. If the correlation coefficient is significant, the flood and nocturnal heat is considered as statistically compound.

Data availability

GPCC is available at https://psl.noaa.gov/data/gridded/data.gpcc.html. ERA5 is available at https://cds.climate.copernicus.eu/cdsapp#!/search?text=ERA5. Homogenized observation data in China can be provided after request to the corresponding author.

Received: 14 June 2024; Accepted: 1 October 2024; Published online: 07 October 2024

References

 Ye, Y. & Qian, C. Conditional attribution of climate change and atmospheric circulation contributing to the record-breaking precipitation and temperature event of summer 2020 in southern China. *Environ. Res. Lett.* 16, 044058 (2021).

- Qian, C., Ye, Y., Bevacqua, E. & Zscheischler, J. Human influences on spatially compounding flooding and heatwave events in China and future increasing risks. Weather Clim. Extremes 42, 100616 (2023).
- Wang, J. et al. Storyline attribution of human influence on a recordbreaking spatially compounding flood-heat event. Sci. Adv. 9, eadi2714 (2023).
- Sadok, W. & Jagadish, S. V. K. The hidden costs of nighttime warming on yields. *Trends Plant Sci.* 25, 644–651 (2020).
- Leonard, M. et al. A compound event framework for understanding extreme impacts. WIREs Clim. Change 5, 113–128 (2014).
- Hurk et al. Analysis of a compounding surge and precipitation event in the Netherlands. Environ. Res. Lett. 10, 035001 (2015).
- Zscheischler, J. & Seneviratne, S. I. Dependence of drivers affects risks associated with compound events. *Environ. Res. Lett.* 3, e1700263 (2017).
- Ridder, N. N. et al. Global hotspots for the occurrence of compound events. Nat. Commun. 11, 5956 (2020).
- Vose, R. S., Easterling, D. R. & Gleason, B. Maximum and minimum temperature trends for the globe: An update through 2004. *Geophys. Res. Lett.* 32, L23822 (2005).
- Sillmann, J. et al. Climate extremes indices in the CMIP5 multimodel ensemble: Part 1. Model evaluation in the present climate. *J. Geophys. Res. Atmos.* 118, 1716–1733 (2013).
- Zhang, P. F. et al. Observed changes in extreme temperature over the global land based on a newly developed station daily dataset. *J. Clim.* 32, 8489–8509 (2019).
- Obradovich, N., Migliorini, R., Mednick, S. C. & Fowler, J. H. Nighttime temperature and human sleep loss in a changing climate. Sci. Adv. 3, e1601555 (2017).
- Tao, J. et al. Daytime and nighttime high temperatures differentially increased the risk of cardiovascular disease: a nationwide hospitalbased study in China. *Environ. Res.* 236, 116740 (2023).
- Zhang, X. et al. Detection of human influence on twentieth-century precipitation trends. *Nature* 448, 461–465 (2007).
- Dunn, R. J. H. et al. Development of an updated global land in situbased data set of temperature and precipitation extremes: HadEX3. J. Geophys. Res. -Atmos. 125, e2019JD032263 (2020).
- IPCC. Climate Change 2021: The physical science basis. In: Masson-Delmotte V., Zhai P., Pirani A., editors. Contribution of Working Group I to the Sixth Assessment Report of the IPCC. Cambridge: Cambridge University Press; 2021.
- Wahl, T. et al. Increasing risk of compound flooding from storm surge and rainfall for major US cities. Nat. Clim. Change 5, 1093–1097 (2015).
- Moftakhari, H. R., Salvadori, G., AghaKouchak, A., Sanders, B. F. & Matthew, R. A. Compounding effects of sea level rise and fluvial flooding. *Proc. Natl Acad. Sci. USA* 114, 9785–9790 (2017).
- Zscheischler, J. et al. Future climate risk from compound events. *Nat. Clim. Change* 8, 469–477 (2018).
- Gershunov, A., Cayan, D. R. & lacobellis, S. F. The great 2006 heat wave over California and Nevada: Signal of an increasing trend. *J. Clim.* 22, 6181–6203 (2009).
- 21. Ha, K. J. & Yun, K. S. Climate change effects on tropical night days in Seoul, Korea. *Theor. Appl. Climatol.* **109**, 191–203 (2012).
- Chen, R., Wen, Z., Lin, W. & Qiao, Y. Diverse relationship between the tropical night in South China and the water vapor transport over the South China Sea and the plausible causes. Atmos. Res. 296, 107080 (2023).
- Zhang, S. & Wang, B. Global summer monsoon rainy seasons. *Int. J. Climatol.* 28, 1563–1578 (2008).
- Adler, R. F., Gu, G. & Huffman, G. Estimating climatological bias errors for the Global Precipitation Climatology Project (GPCP). J. Appl. Meteorol. Climatol. 51, 84–99 (2012).
- Adler, R. F. et al. Global precipitation: means, variations and trends during the satellite era (1979–2014). Surv. Geophys. 38, 679–699 (2017).
- 26. Liu, Y. & Wu, G. Progress in the study on the formation of the summertime subtropical anticyclone. *Adv. Atmos. Sci.* **21**, 322–342 (2004).

- Wei, Y. et al. Impact of North Indian atmospheric diabatic heating on summer precipitation in Central Asia. J. Clim. 36, 4345–4362 (2023).
- Higgins, R. W. et al. Influence of the Great Plains low-level jet on summertime precipitation and moisture transport over the central United States. J. Clim. 10, 481–507 (1997).
- Chen, R., Wen, Z. & Lu, R. Interdecadal change on the relationship between the mid-summer temperature in South China and atmospheric circulation and sea surface temperature. Clim. Dyn. 54, 2113–2126 (2018).
- Li, X. et al. Decadal transition of the leading mode of interannual moisture circulation over East Asia—western North Pacific: Bonding to different evolution of ENSO. J. Clim. 32, 289–308 (2019).
- Qu, X. & Huang, G. An enhanced influence of tropical Indian Ocean on the South Asia High after the late 1970s. J. Clim. 25, 6930–6941 (2012).
- Weaver, S., Shubert, S. & Wang, H. Warm season variations in the low-level circulation and precipitation over the central United States in observations, AMIP simulations, and idealized SST experiments. *J. Clim.* 22, 5401–5420 (2009).
- Chen, W., Lu, R. & Ding, H. A decadal intensification in the modulation of spring western tropical Atlantic sea surface temperature to the following winter ENSO after the mid-1980s. Clim. Dyn. 59, 3643–3655 (2022).
- Klein, J. A., Harte, J. & Zhao, X. Experimental warming, not grazing, decreases rangeland quality on the Tibetan plateau. *Ecol. Appl.* 17, 541–557 (2007).
- Wang, S. et al. Effects of warming and grazing on soil N availability, species composition, and ANPP in an alpine meadow. *Ecology* 93, 2365–2376 (2012).
- Ma, Z. et al. Climate warming reduces the temporal stability of plant community biomass production. *Nat. Commun.* 8, 15378 (2017).
- Chen, H. et al. The impacts of climate change and human activities on biogeochemical cycles on the Qinghai-Tibetan Plateau. *Glob. Change Biol.* 19, 2940–2955 (2013).
- 38. Allan, R. P. et al. Physically consistent responses of the global atmospheric hydrological cycle in models and observations. *Surv. Geophys.* **35**, 533–552 (2014).
- Kim, S. et al. Linking total precipitable water to precipitation extremes globally. Earths Fut. 10, e2021EF002473 (2020).
- AghaKouchak, A. et al. Climate extremes and compound hazards in a warming world. Annu. Rev. Earth Planet. Sci. 48, 519–548 (2020).
- 41. Pfahl, S., O'Gorman, P. A. & Fischer, E. M. Understanding the regional pattern of projected future changes in extreme precipitation. *Nat. Clim. Change* **7**, 423–427 (2017).
- Allan, R. P. et al. Advances in understanding large-scale responses of the water cycle to climate change. *Ann. N. Y. Acad. Sci.* 1472, 49–75 (2020).
- 43. Bevacqua, E. et al. Higher probability of compound flooding from precipitation and storm surge in Europe under anthropogenic climate change. *Sci. Adv.* **5**, eaaw5531 (2019).
- 44. Li, W. et al. Anthropogenic impact on the severity of compound extreme high temperature and drought/rain events in China. *npj Clim. Atmos. Sci.* **6**, 79 (2023).
- 45. Shepherd, T. G. Atmospheric circulation as a source of uncertainty in climate change projections. *Nat. Geosci.* **7**, 703–708 (2014).
- Smith, D. M. et al. North Atlantic climate far more predictable than models imply. *Nature* 583, 796–800 (2020).
- 47. O'Reilly, C. H. et al. Projections of northern hemisphere extratropical climate underestimate internal variability and associated uncertainty. *Commun. Earth Environ.* **2**, 194 (2021).
- Li, Z. et al. A comparative analysis of changes in temperature and precipitation extremes since 1960 between China and Greece. Atmosphere 13, 1824 (2022).
- Schneider, U. et al. Evaluating the hydrological cycle over land using the newly-corrected precipitation climatology from the Global Precipitation Climatology Centre (GPCC). Atmosphere 8, 52 (2017).
- Hersbach, H., et al. ERA5 monthly averaged data on pressure levels from 1940 to present. Copernicus Climate Change Service (C3S)

- Climate Data Store (CDS), https://doi.org/10.24381/cds.6860a573 (2023).
- 51. IPCC. Managing the risks of extreme events and disasters to advance climate change adaptation. In: Field, C. B., Barros, V., Stocker, T. F. editors. A Special Report of Working Groups I and II of the Intergovernmental Panel on Climate Change. Cambridge: Cambridge University Press; 2012.
- 52. Jézéquel, A., Yiou, P. & Radanovics, S. Role of circulation in European heatwaves using flow analogues. *Clim. Dyn.* **50**, 1145–1159 (2018).

Acknowledgements

This study is supported by the National Natural Science Foundation of China (42375028, U2342205), and the Science and Technology Planning Project of Guangdong Province (2023B1212060019).

Author contributions

R. Chen designed the research. All authors wrote the code, conducted calculations, produced the figures and interpreted the results. R. Chen wrote the manuscript and all authors reviewed the manuscript.

Competing interests

The authors declare no competing interests.

Additional information

Supplementary information The online version contains supplementary material available at https://doi.org/10.1038/s41612-024-00795-y.

Correspondence and requests for materials should be addressed to Ruidan Chen.

Reprints and permissions information is available at http://www.nature.com/reprints

Publisher's note Springer Nature remains neutral with regard to jurisdictional claims in published maps and institutional affiliations.

Open Access This article is licensed under a Creative Commons Attribution-NonCommercial-NoDerivatives 4.0 International License, which permits any non-commercial use, sharing, distribution and reproduction in any medium or format, as long as you give appropriate credit to the original author(s) and the source, provide a link to the Creative Commons licence, and indicate if you modified the licensed material. You do not have permission under this licence to share adapted material derived from this article or parts of it. The images or other third party material in this article are included in the article's Creative Commons licence, unless indicated otherwise in a credit line to the material. If material is not included in the article's Creative Commons licence and your intended use is not permitted by statutory regulation or exceeds the permitted use, you will need to obtain permission directly from the copyright holder. To view a copy of this licence, visit http://creativecommons.org/licenses/bync-nd/4.0/.

© The Author(s) 2024